Passive suppression of helicopter ground resonance using nonlinear energy sinks attached on the helicopter blades

Baptiste Bergeot, Sergio Bellizzi, Bruno Cochelin

Passive suppression of helicopter ground resonance using nonlinear energy sinks attached on the helicopter blades

B. Bergeot[1,2,*], S. Bellizzi[2] and B. Cochelin[2]

[1] *INSA Centre Val de Loire, Université François Rabelais de Tours, LMR EA 2640, Campus de Blois, 3 Rue de la Chocolaterie, CS 23410, 41034 Blois Cedex, France*

[2] *Aix Marseille Univ, CNRS, Centrale Marseille, LMA, 4 impasse Nikola Tesla 13453 Marseille Cedex 13, France*

[*] *Corresponding author:* baptiste.bergeot@insa-cvl.fr

Abstract

This paper investigates the passive control of a rotor instability named helicopter Ground Resonance (GR). The passive device consists of a set of essential cubic nonlinear absorbers named Nonlinear Energy Sinks (NES) each of them positioned on a blade. A dynamic model reproducing helicopter GR instability is presented and transformed to a time-invariant nonlinear system using a multi-blade coordinate transformation based on Fourier transform mapping the dynamic state variables into a non-rotating reference frame. Combining complexification, slow/fast partition of the dynamics and averaging procedure, a reduced model is obtained allowed us to use the so-called geometric singular perturbation analysis to characterize the steady state response regimes. As in the case of a NES attached to the fuselage, it is shown that under suitable conditions, GR instability can be completely suppressed, partially suppressed through periodic response or strongly modulated response. Relevant analytical results are compared, for validation purposes, to direct integration of the reference and reduced models.

Keywords: Helicopter ground resonance ; Passive control ; Nonlinear energy sink ; Complex multi-blade coordinate transformation ; Relaxation oscillations ; Strongly modulated response

1 Introcuction

A Nonlinear Energy Sink (NES) is a passive nonlinear absorber which introduces non linear coupling between the main structure and the absorber for controlling the vibratory response of the structure under external excitation. A NES consists on a nonlinear oscillator with an essentially nonlinear restoring force and generally a small mass compared to the main structure. The objective of the NES is to capture the energy of the main structure and to dissipate it. This is done through the Targeted Energy Transfer (TET) concept. TET is based on the capacity of the essential nonlinear oscillator to be resonant at any frequencies giving possible tuning with the main structure to be controlled. TET has been widely studied in the literature [1, 2, 3, 4].

NES also represents an alternative device for control systems with self-excitation. The possible suppression of the limit cycle oscillations of a van der Pol oscillator coupled to a NES is demonstrated numerically in [5] and the self-excitation response regimes are investigated theoretically in [6] where an asymptotic analysis of the system related to slow/super-slow decomposition of the averaged flow reveals periodic responses, global bifurcations of different types and basins of attraction of various self-excitation regimes. A series of papers [7, 8, 9, 10] are dedicated to aeroelastic

instability. It is demonstrated that a NES coupled to a rigid wing in subsonic flow can partially or even completely suppress aeroelastic instability. The suppression mechanisms are investigated numerically in [7] and [9] for one and multi-DOF NES. Several aspects of the suppression mechanisms are validated expermentally in [8]. Finally an asymptotic analysis is reported in [10] demonstrating the existence of the three passive suppression mechanisms based on TET. Suppression of aeroelastic instability of a long span bridge model is also considered in [11] whereas [12] is dedicated to a general class of nonlinear multi degree of freedom system including aeroelastic forces. In [13, 14] it is shown that a NES is able to quench chatter instability in turning process whereas in [15] the stabilization of drill-string systems is considered. Note that in [16], it is demonstrated that a nonlinear tuned vibration absorber possessing a linear spring and a nonlinear spring whose mathematical form is determined according the nonlinearity in the host system can suppress limit cycle oscillations.

In this paper, we focus on the instability in helicopter rotor named Ground Resonance (GR) problem. GR is related to the coupling of the rotor blade in-plane motion with the airframe motion on its landing gear. The standard reference of the GR analysis is the paper by Coleman and Feingold [17] where it is established, considering an isotropic rotor, that GR is due to a frequency coalescence between a lag mode and the fuselage mode. The range of rotor speeds for which this frequency coalescence occurs is predicted analytically. More references can be found in [18, 19, 20, 21] and a recent analysis of helicopter GR with asymmetric blades can be found in [22]. Traditionally, GR instability is prevented by increasing damping in the landing gear and blades [23, 24]. A robustness analysis is discussed in [25]. Active control of GR has been also studied in [21].

The initial application of a NES to control GR instability was considered in [26, 27]. A theoretical/numerical analysis of the steady-state responses of a helicopter model with a minimum number of degrees of freedom that can reproduce Helicopter Ground Resonance instability when a NES is attached on the fuselage in an ungrounded configuration was performed. The system was first simplified using successively Coleman transformation [17] and binormal transformation [23] followed by a complexification-averaging method together with geometric singular perturbation. Four steady-state responses are highlighted and explained analytically: complete suppression, partial suppression through strongly modulated response, partial suppression through periodic response and no suppression of the Helicopter Ground Resonance.

In this study, the same problem is considered but now the NES on the fuselage is removed and it is replaced by a set of NES, each of them been positioned on a blade. A similar configuration has been considered in [28, 29] where the efficiency of NES on rotating part of a rotor has been analyzed under mass eccentricity force [28] and under an external forcing [29]. One of the advantages of this configuration is to reduce the weight due to the additional absorbers. Here, response regimes are investigated extending the theoretical/numerical analysis developed in [26] using a Fourier coordinate transformation as in [30]. In contrast to the Colman transformation, this multi-blade coordinate transformation can be easily combined with the complexification-averaging method together with geometric singular perturbation.

The next section introduces the helicopter model including a fuselage and four blades with a NES attached on each blade. Only one direction of the fuselage motion, the lag motion of each blade and the lag motion of each associated NES are considered. Based on Fourier coordinate transform, the model is reduced to a time-invariant nonlinear system involving complex variables. In Sect. 3, linear stability analysis is performed on this reduced model showing that this model is able to reproduce GR phenomenon. In Sect. 4, the analytical procedure [26] based on averaging method together with geometric singular perturbation theory is adapted to the reduced system. It is shown that it is able to characterize the situations for which trivial solution is unstable. In Sect. 5, numerical analysis is performed and discussed considering analytical results validated from direct integration of the reference model and the reduced model. Finally in Sect. 6, few words

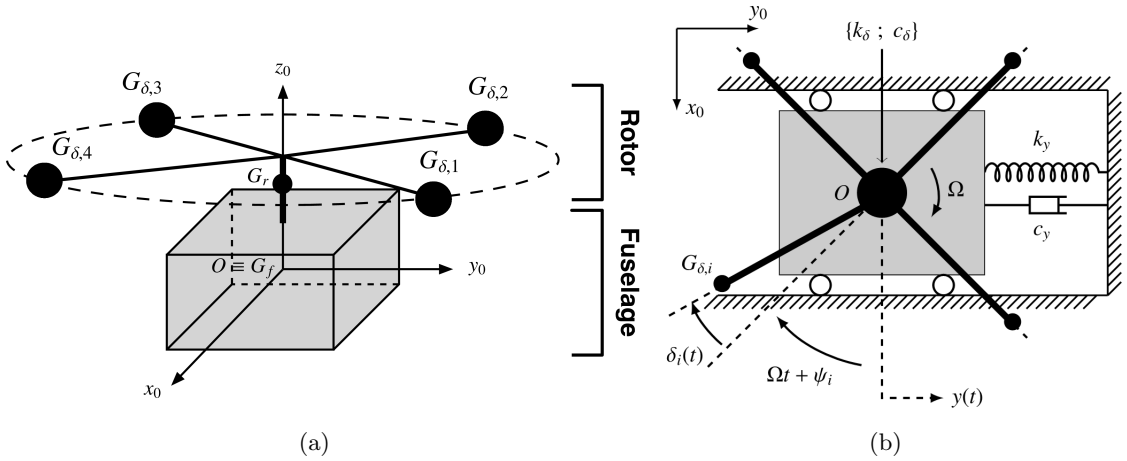

Figure 1: Descriptive diagram of the used helicopter system. (a) Overview of the system. (b) View from the top.

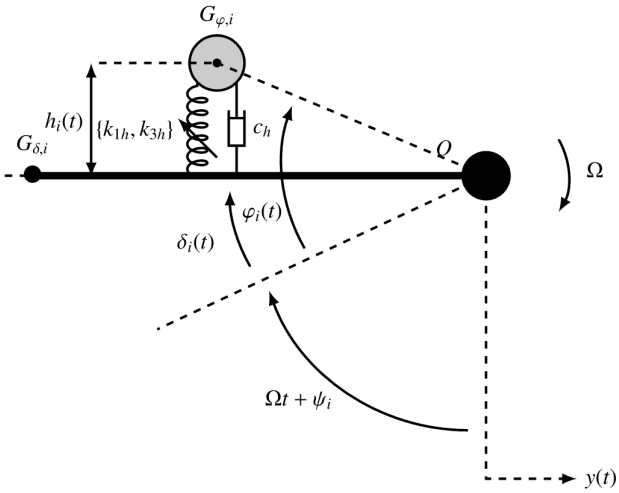

Figure 2: Descriptive diagram of the NES attachment on the i-th blade. The length $[OG_{\varphi,i}]$ is called L_φ.

about the comparison between blade and fuselage NES attachments are expounded.

2 The model

2.1 Initial equations of motion

The helicopter model studied is shown Fig. 1. It consists of a fuselage and a 4-blades rotor rotating at a constant speed Ω. This model is very similar to that described for example in [18, 19, 21].

The fuselage is a simple mass-spring damped system with mass m_y, spring constant k_y, viscous damper of damping coefficient c_y and the translational DOF y. It is assumed that the center of inertia G_f of the fuselage at rest coincides with the origin O of the earth-fixed system of coordinates (O, x_0, y_0, z_0). Each blade is assumed to be a point mass $G_{\delta,i}$ (with $i \in [1, 4]$) with mass m_δ linked to the axis (O, z_0) with a bar without mass of length L_δ and an articulation with torsional spring k_δ and viscous damper of damping coefficient c_δ. Only lag motions of the blades, characterized by the lag angle δ_i (with $i \in [1, 4]$), are taken into account.

This simple model is used to study the effect of attaching a NES in ungrounded configuration on each blade of the helicopter (as shown Fig. 2) in order to control lagging motion and consequently ground resonance instability.

Each NES is a nonlinear-spring mass damped system (see Fig. 2) with mass m_h at the mass point $G_{\varphi,i}$ (with $i \in [1,4]$), linear spring constant k_{1h}, cubic spring constant k_{3h}, and viscous damper of damping coefficient c_h. Each NES is placed at distance L_φ from the axis (O, z_0) and it is characterized with only the lag angle DOF φ_i which is related to the relative displacement h_i by $h_i = L_\varphi \sin(\varphi_i - \delta_i)$.

Starting from the position of the center of inertia and the corresponding velocity of the i-th blade (respectively the i-th NES) in the plane (O, x_0, y_0), defined as

$$OG_{\delta,i} = \begin{pmatrix} L_\delta \cos\left(\Omega t + \psi_i + \delta_i\right) \\ y + L_\delta \sin\left(\Omega t + \psi_i + \delta_i\right) \end{pmatrix}, \tag{1}$$

and,

$$v_{\delta,i} = \begin{pmatrix} -L_\delta \left(\Omega + \dot{\delta}_i\right) \sin\left(\Omega t + \psi_i + \delta_i\right) \\ \dot{y} + L_\delta \left(\Omega + \dot{\delta}_i\right) \cos\left(\Omega t + \psi_i + \delta_i\right) \end{pmatrix}, \tag{2}$$

and,

$$OG_{\varphi,i} = \begin{pmatrix} L_\varphi \cos\left(\Omega t + \psi_i + \varphi_i\right) \\ y + L_\varphi \sin\left(\Omega t + \psi_i + \varphi_i\right) \end{pmatrix}, \tag{3}$$

$$v_{\varphi,i} = \begin{pmatrix} -L_\varphi \left(\Omega + \dot{\varphi}_i\right) \sin\left(\Omega t + \psi_i + \varphi_i\right) \\ \dot{y} + L_\varphi \left(\Omega + \dot{\varphi}_i\right) \cos\left(\Omega t + \psi_i + \varphi_i\right) \end{pmatrix} \tag{4}$$

with,

$$\psi_i = -\frac{\pi}{2}(i-1) \tag{5}$$

the equations of motion of the whole system is derived using Lagrange equations from the kinetic energy T, the potential energy V and the Rayleigh dissipation function D written as

$$T = \frac{1}{2} m_y \dot{y}^2 + \sum_{i=1}^{4} \frac{1}{2} m_\delta v_{\delta,i}^2 + \sum_{i=1}^{4} \frac{1}{2} m_\varphi v_{\varphi,i}^2, \tag{6}$$

$$V = \frac{1}{2} k_y y^2 + \sum_{i=1}^{4} \frac{1}{2} k_\delta \delta_i^2 + \sum_{i=1}^{4} \frac{1}{2} k_1 \sin^2(\varphi_i - \delta_i) + \sum_{i=1}^{4} \frac{1}{4} k_3 \sin^4(\varphi_i - \delta_i), \tag{7}$$

$$D = \frac{1}{2} c_y \dot{y}^2 + \sum_{i=1}^{4} \frac{1}{2} c_\delta \dot{\delta}^2 + \sum_{i=1}^{4} \frac{1}{2} c_\varphi \sin^2(\dot{\varphi}_i - \dot{\delta}_i), \tag{8}$$

with $k_1 = L_\varphi^2 k_{1h}$, $k_3 = L_\varphi^4 k_{3h}$ and $c_\varphi = L_\varphi^2 c_h$.

Assuming small angles ($|\varphi_i| \ll 1$ and $|\delta_i| \ll 1$) and also small angle differences ($|\varphi_i - \delta_i| \ll 1$, the equations of motion reduce to a nonlinear differential system with periodic coefficient

$$\begin{cases} \left(m_y + 4(m_\delta + m_\varphi)\right) \ddot{y} + c_y \dot{y} + k_y y \\ + M_\delta \sum_{i=1}^{4} \left\{ \left(\ddot{\delta}_i - \Omega^2 \delta_i\right) \cos\left(\Omega t + \psi_i\right) - 2\Omega \dot{\delta}_i \sin\left(\Omega t + \psi_i\right) \right\} \\ + M_\varphi \sum_{i=1}^{4} \left\{ \left(\ddot{\varphi}_i - \Omega^2 \varphi_i\right) \cos\left(\Omega t + \psi_i\right) - 2\Omega \dot{\varphi}_i \sin\left(\Omega t + \psi_i\right) \right\} = 0 & \text{(9a)} \\ I_\delta \ddot{\delta}_i + c_\delta \dot{\delta}_i + c_\varphi(\dot{\delta}_i - \dot{\varphi}_i) + k_\delta \delta_i + k_1 \left(\delta_i - \varphi_i\right) + k_3 \left(\delta_i - \varphi_i\right)^3 + M_\delta \ddot{y} \cos\left(\Omega t + \psi_i\right) = 0, \quad i = 1,4 & \text{(9b)} \\ I_\varphi \ddot{\varphi}_i - c_\varphi(\dot{\delta}_i - \dot{\varphi}_i) - k_1 \left(\delta_i - \varphi_i\right) - k_3 \left(\delta_i - \varphi_i\right)^3 + M_\delta \ddot{y} \cos\left(\Omega t + \psi_i\right) = 0, \quad i = 1,4. & \text{(9c)} \end{cases}$$

where "$\dot{}$" denotes the derivative with respect to time t and $M_\delta = m_\delta L_\delta$ and $I_\delta = m_\delta L_\delta^2$ (respectively $M_\varphi = m_\varphi L_\varphi$ and $I_\varphi = m_\varphi L_\varphi^2$) are the static moment and the moment of inertia of each blade (respectively NES).

It is important to note that the cosine and sine functions do not now depend on the angle variables δ_i and φ_i (see for the record Eqs. (1)-(4)) as the result of the small angle assumption (all the cosine and sine terms have been expanded in a first-order Taylor series around the trivial equilibrium position).

2.2 Scaled equations of motion: the Reference Model (RefM)

Our objective is to show that the lightweight ungrounded NES can be effective passive absorbers and local energy dissipators to mitigate instabilities.

Defining the lightweight of a NES with respect to a blade as the ratio of the moments of inertia

$$\epsilon = \frac{I_\varphi}{I_\delta}. \tag{10}$$

and introducing the barycentric coordinates $v_i(t)$ and $w_i(t)$ as

$$v_i = \delta_i + \epsilon\,\varphi_i \qquad \text{and} \qquad w_i = \delta_i - \varphi_i, \qquad \text{for} \qquad i = 1, \cdots, 4, \tag{11}$$

Eqs. (9) become

$$\begin{cases} \ddot{y} + \epsilon\lambda_y\dot{y} + \omega_y^2 y + \dfrac{1}{2(1+\epsilon)}\displaystyle\sum_{i=1}^{4}\Bigg\{ & \text{(12a)} \\ \epsilon\Omega\sin(\Omega t + \psi_i)\,\Big(-(S_d+\epsilon T_d)(\Omega + \epsilon\Omega + 2\dot{v}_i) + 2\epsilon(T_d - S_d)\dot{w}_i\Big) & \\ +\epsilon\cos(\Omega t + \psi_i)\Big((S_d+\epsilon T_d)(\ddot{v}_i - \Omega^2 v_i) - \epsilon(T_d - S_d)(\ddot{w}_i - \Omega^2 w_i)\Big)\Bigg\} = 0 & \text{(12b)} \\ \ddot{v}_i + \epsilon\lambda_\delta\dfrac{\dot{v}_i + \epsilon\dot{w}_i}{\epsilon+1} + \omega_\delta^2\dfrac{v_i + \epsilon w_i}{\epsilon+1} + & \\ \qquad \epsilon(S_c + \epsilon T_c)\ddot{y}\cos(\Omega t + \psi_i) = 0,\ i = 1, 4 & \text{(12c)} \\ \ddot{w}_i + \epsilon\lambda_\delta\dfrac{\dot{v}_i + \epsilon\dot{w}_i}{\epsilon+1} + \omega_\delta^2\dfrac{v_i + \epsilon w_i}{\epsilon+1} - \epsilon(T_c - S_c)\ddot{y}\cos(\Omega t + \psi_i) & \\ +\mu(1+\epsilon)\dot{w} + \alpha_1(1+\epsilon)w_i + \alpha_3(1+\epsilon)w_i^3 = 0,\ i = 1, 4 & \text{(12d)} \end{cases}$$

where the following notations defining rescaled parameters

$$\omega_y^2 = k_y/\left(m_y + 4(m_\delta + m_\varphi)\right), \tag{13a}$$
$$\omega_\delta^2 = k_\delta/I_\delta, \tag{13b}$$
$$\epsilon\lambda_y = c_y/\left(m_y + 4(m_\delta + m_\varphi)\right), \tag{13c}$$
$$\epsilon\lambda_\delta = c_\delta/I_\delta, \tag{13d}$$
$$\epsilon\mu = c_\varphi/I_\delta, \tag{13e}$$
$$\epsilon\alpha_1 = k_1/I_\delta, \tag{13f}$$
$$\epsilon\alpha_3 = k_3/I_\delta, \tag{13g}$$
$$\epsilon S_c = M_\delta/I_\delta = 1/L_\delta, \tag{13h}$$
$$\epsilon^2 T_c = M_\varphi/I_\delta, \tag{13i}$$

$$\epsilon S_d = 2M_\delta / \left(m_y + 4(m_\delta + m_\varphi)\right), \tag{13j}$$
$$\epsilon^2 T_d = 2M_\varphi / \left(m_y + 4(m_\delta + m_\varphi)\right), \tag{13k}$$

have been used.

In the sequel, we will be assumed that $\epsilon \ll 1$ with λ_y, λ_δ, μ, α_1, α_3, S_d, T_d ,S_c, $T_c \sim O(1)$. We point that expression (13i) defining $M_\varphi/I_\delta = \epsilon/L_\varphi$ is already of the order of ϵ. In the same way, if we reason with scaled parameters $\tilde{S}_d = 2M_\delta/\left(m_y + 4(m_\delta + m_\varphi)\right)$ and $\tilde{T}_d = 2M_\varphi/\left(m_y + 4(m_\delta + m_\varphi)\right)$, therefore, $\tilde{T}_d = \tilde{S}_d\left(M_\varphi/M_\delta\right) = \tilde{S}_d\epsilon\left(L_\delta/L_\varphi\right) = S_d\epsilon^2\left(L_\delta/L_\varphi\right)$. Therefore, ϵ^2 appears in Eqs. (13i) and (13k) resulting of the assumption that the lengths L_δ and L_φ are the same order of magnitude. Eqs. (12) defines the Reference Model (RefM).

2.3 The time-invariant system

To develop an analytic method for characterizing the motions of the helicopter when Ground Resonance (GR) can occur, RefM has to be reduced (and/or simplified) to a time-invariant system. Classically, a Coleman transform [17] is used. Coleman transform consists in a change of variables which transforms individual motions of the blades (described by the lagging angles) into collective motions described by the so-called Coleman coordinates. Coleman transform applied to a linear system with periodic coefficients gives a linear system with constant coefficients.

Here a complex transformation, first proposed in [30] and used for example in [28], is preferred to Coleman transform because this complex transformation deals easily with nonlinearities. Indeed, we can first work in the rotating reference frame applying the following complex transformation of the variables v_i and w_i (for $i = 1$ to 4)

$$v_i(t) = \sum_{k=0}^{4-1} a_k(t) e^{-jk\psi_i}, \text{ with } i = 1, \cdots, 4 \tag{14}$$

given equivalently

$$a_k(t) = \frac{1}{4}\sum_{i=1}^{4} v_i(t) e^{jk\psi_i}, \text{ with } k = 0, \cdots, 3 \tag{15}$$

and,

$$w_i(t) = \sum_{k=0}^{4-1} b_k(t) e^{-jk\psi_i}, \text{ with } i = 1, \cdots, 4 \tag{16}$$

given equivalently

$$b_k(t) = \frac{1}{4}\sum_{i=1}^{4} w_i(t) e^{jk\psi_i}, \text{ with } k = 0, \cdots, 3 \tag{17}$$

with $j^2 = -1$. The new variable a_k and b_k (for $k = 0$ to 3), called modal coordinates, are now complex and satisfy the following relations $a_{4-k} = a_k^*$ and $b_{4-k} = b_k^*$ where " * " is the usual notation for the complex conjugate.

Substituting Eqs. (14) and (16) into Eqs. (12), it can be observed that the modal coordinates a_0 and a_2 are uncoupled from a_1, a_3, b_1, b_3 and the rotor lateral vibration y. Moreover the modal coordinates b_0 and b_2 are linearly uncoupled from a_1, a_3, b_1, b_3 and the rotor lateral vibration y. In a linear approximation, the components a_0, a_2, b_0 and b_2 are neglected. Recalling that $a_3 = a_1^*$ and $b_3 = b_1^*$, we therefore consider only the equations of motion associated to y, a_1 and b_1. For convenience, variables a_1 and b_1 are now noted simply a and b.

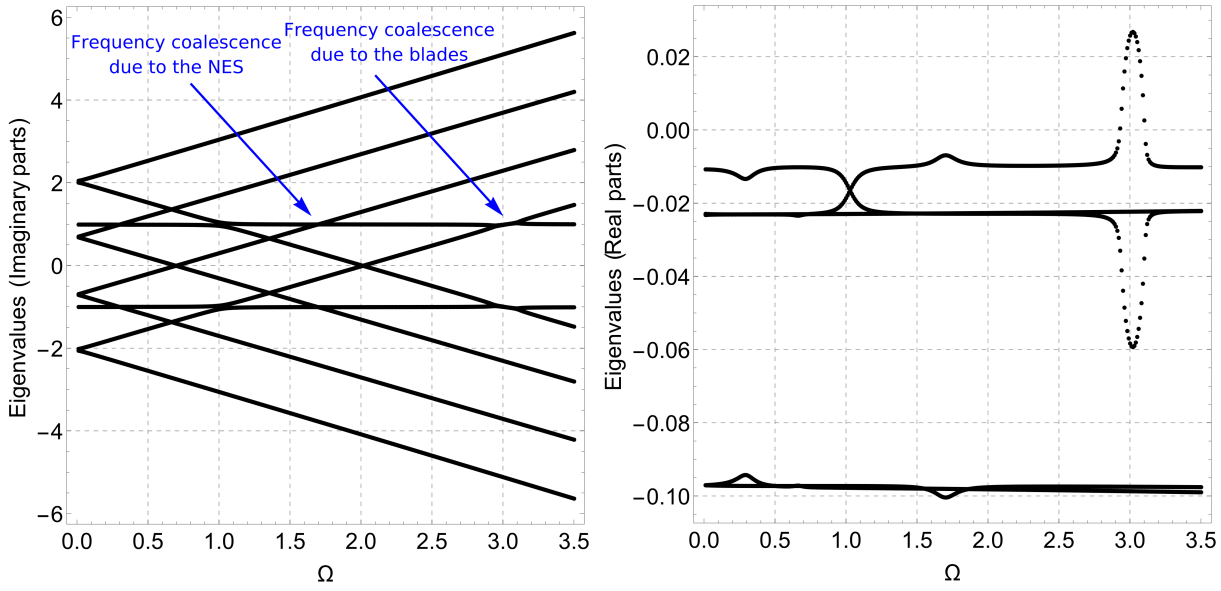

(a) (b)

Figure 3: Evolution of imaginary (a) and real (b) parts of the eigenvalues of the vector function $\mathbf{F_1}$ evaluated at the trivial equilibrium. Parameters used: $\lambda_y = 0.2$, $\omega_y = 1$, $S_d = 1$, $T_d = 0.1$, $S_c = 3$, $T_c = 1$, $\lambda = 0.2$, $\omega_\delta = 2$, $\mu = 0.2$, $\alpha_1 = 0.5$ and $\epsilon = 0.1$.

Finally, equations of motion are written in the inertia reference frame using the variables A and B defined as follow

$$A(t) = a(t)e^{j\Omega t} \qquad \text{and} \qquad B(t) = b(t)e^{j\Omega t}. \tag{18}$$

where A and B are also complex variables. The equations of motion associated to y, A and B reduce to

$$\begin{cases} \ddot{y} + \epsilon\lambda_y\dot{y} + \omega_y^2 y + \epsilon\dfrac{S_d + \epsilon T_d}{1+\epsilon}\left(\ddot{A} + \ddot{A}^*\right) + \epsilon^2\dfrac{S_d - T_d}{1+\epsilon}\left(\ddot{B} + \ddot{B}^*\right) = 0 & \text{(19a)} \\ \ddot{A} + \left(\dfrac{\epsilon\lambda_\delta}{1+\epsilon} - 2j\Omega\right)\dot{A} + \dfrac{-\Omega(\Omega + \epsilon(i\lambda_\delta + \Omega)) + \omega_\delta^2}{1+\epsilon}A + \dfrac{1}{2}\epsilon\left(S_c + T_c\epsilon\right)\ddot{y} + \dfrac{\epsilon^2\lambda_\delta}{1+\epsilon}\dot{B} + \epsilon\dfrac{-j\epsilon\lambda_\delta\Omega + \omega_\delta^2}{1+\epsilon}B & \text{(19b)} \\ \ddot{B} + \left(\mu - 2j\Omega + \epsilon\left(\mu + \dfrac{\lambda_\delta\epsilon}{\epsilon+1}\right)\right)\dot{B} + \dfrac{\alpha_1(1+\epsilon)^2 + \Omega\left(-j\left(\epsilon^2\lambda_\delta + (1+\epsilon)^2\mu\right) - (1+\epsilon)\Omega\right) + \epsilon\omega_\delta^2}{1+\epsilon}B \\ \quad + \dfrac{1}{2}(S_c - T_c)\epsilon\ddot{y} + \dfrac{\epsilon\lambda_\delta}{1+\epsilon}\dot{A} + \dfrac{-j\epsilon\lambda_\delta\Omega + \omega_\delta^2}{1+\epsilon}A + 3\alpha_3(1+\epsilon)\left|B\right|^2 B = 0. & \text{(19c)} \end{cases}$$

High harmonic terms in $e^{4jt\Omega}$ appearing in Eqs. (19c) have been ignored. The resulting equations are now time-invariant system of equations. They will be used to perform linear stability analysis of the trivial solution and also as starting point of the nonlinear analysis.

3 Preliminary results

3.1 Ground resonance analysis

Helicopter ground resonance is a consequence of a dynamic instability which appears in the RefM for given values of the rotor speed Ω. Considering the time-variant (or parametrically excited) systems (9) or (12) the instability is a *parametric combination resonance of the summed type*, see e.g. [31]. This king of instability can be analyzed using classical methods for linear time-variant ordinary differential equations as Floquet theory, see e.g. [31, 32]. However, is it easier (and equivalent) to perform the stability analysis on the time-invariant system (19) in which the instability becomes a mode coupling instability. Usually, the ground resonance phenomenon is analyzed on a time-invariant system resulting of Coleman transformation (see [18] for more details) instead of the used complex transformation defined by Eqs. (14-17).

It is easy to show that the only fixed point of Eqs. (19) is the trivial solution $y = A = A^* = B = B^* = 0$. As usual, stability of the fixed point is found by looking the sign of the eigenvalues real parts of the Jacobian matrix of the vector function $\mathbf{F_1}$ evaluated at the trivial equilibrium. The vector function $\mathbf{F_1}$ characterizes the system of Eqs. (19) when it is formally written in state-space form

$$\dot{\mathbf{U}} = \mathbf{F_1}\left(\mathbf{U}\right), \text{ with } \mathbf{U} = \left[y\ A\ A^*\ B\ B^*\ \dot{y}\ \dot{A}\ \dot{A}^*\ \dot{B}\ \dot{B}^*\right]^t. \tag{20}$$

The evolution, with respect to the rotor speed Ω, of the 10 complex conjugates eigenvalues of the Jacobian matrix of the vector function $\mathbf{F_1}$ are plotted in Fig. 3. Near $\Omega = \omega_y + \omega_\delta$, a phenomenon of frequency coalescence is observed, the real part of one of the eigenvalues becomes positive and a dynamic instability occurs; this is the helicopter ground resonance. Due to the presence of the NES attachments, a second frequency coalescence appears near $\Omega = \omega_y + \sqrt{\alpha_1} \approx 1.7$. This can be a problem if one wants to build such a device. However, the assumption that the lengths L_δ and L_φ are the same order of magnitude leading to Eq. (13k) implies a weak coupling between the NES and the fuselage. As a result, in this situation, this frequency coalescence does not produce a dynamic instability. Indeed, no real part of the eigenvalues become positive (see Fig. 3(b)).

3.2 Some steady-state response regimes

Using numerical integration of the RefM, Eqs. (12), four different types of response regimes which may be highlighted. They are classified into two categories depending on the fact that the trivial solution of the RefM, calculated in Sect. 3.1, is stable or not:

- **The trivial solution of the RefM is stable:**
  - *Complete suppression.* In this case, the additional damping due to the NES attachment stabilizes the system and the GR instability is completely suppressed.
- **The trivial solution of RefM is unstable**:
  - *Partial suppression through Periodic Response (PR).* In this case, the steady-state response regime is periodic with frequency close to ω_y[1].
  - *Partial suppression through Strongly Modulated Response (SMR).* In this case, the steady-state response regime is a quasiperiodic regime which exhibits a "fast" component with frequency close to ω_y and a "slow" component corresponding to the envelope of the signal. The term "Strongly modulated response" has been introduced by Starosvetsky and Gendelman [4] for the study of a harmonic forced linear system coupled to a NES.

[1] This can be shown for example by computing the power spectrum of the steady part of the signal.

– *No suppression of GR.* The NES is not able to maintain stable steady-state regimes. We observe exponential growth of the system.

These four responses are also observed by Bergeot et al. [26] when one NES is attached on the fuselage of the helicopter.

4 Theoretical study: asymptotic analysis

Our objective is to develop a similar procedure as in Bergeot et al. [26] to characterize the periodic solution with period ω_y for Ω in the neighborhood of $\omega_y + \omega_\delta$. The proposed method combines reduction by *complexfication-averaging* (CA-X) procedure [33, 3] and analysis using *geometric singular perturbation theory* (GSPT) [34, 35, 36].

4.1 The slow-flow

Starting from Eqs. (19), complexification[2] can be achieved re-writing the variable y as

$$\xi = \dot{y} + j\omega_y y, \tag{21}$$

giving reciprocally,

$$y = \frac{\xi - \xi^*}{2j\omega_y}, \qquad \dot{y} = \frac{\xi + \xi^*}{2} \qquad \text{and} \qquad \ddot{y} = \dot{\xi} - \frac{j\omega_y}{2}\left(\xi + \xi^*\right). \tag{22}$$

Then, averaging method is developed in the way of the *complexification-averaging method* first introduced by Manevitch [33] and discussed in detail by Vakakis et al. [3]. Only the main steps are given here after.

We assume that the variable ξ, A and B may be broken down into fast and slow components introducing the following representation

$$\xi_1 = \phi_1(\tau)e^{j\omega_y t}\,, \qquad A = \phi_2(\tau)e^{j\omega_y t}\,, \qquad B = \phi_3(\tau)e^{j\omega_y t}, \tag{23}$$

where $\tau = \epsilon t$ (τ defines the *super-slow* time scale, see hereafter for more details about this designation) and ϕ_i (with $i \in [1, 3]$) is the complex slow modulated amplitude of the fast component $e^{j\omega_y t}$.

The following steps are performed to obtain the slow flow of Eqs. (19):

1. Eqs. (22) and (23) are substituted into Eqs. (19);
2. An averaging over one period of the frequency ω_y is performed;
3. The resulting equations are written with respect to the super-slow time scale, taking into account the fact that

$$\frac{d\phi_i(\tau)}{dt} = \epsilon\frac{d\phi_i(\tau)}{d\tau} \qquad \text{and} \qquad \frac{d^2\phi_i(\tau)}{dt^2} = \epsilon^2\frac{d\phi_i(\tau)}{d\tau^2}, \tag{24}$$

4. The equations are rewritten with respect to the slow time scale t;
5. A first-order Taylor series around $\epsilon = 0$ is performed.

[2] The complexification is not necessary for the variable $A(t)$ and $B(t)$ because they are already complex variables.

Finally, Eqs. (19) are reduced as

$$\begin{cases} \dot{\phi}_1 = \epsilon f_1\left(\phi_1, \phi_2, \phi_3\right) & \text{(25a)} \\ \dot{\phi}_2 = \epsilon f_2\left(\phi_1, \phi_2, \phi_3\right) & \text{(25b)} \\ \dot{\phi}_3 = f_3\left(\phi_1, \phi_2, \phi_3, \epsilon\right) & \text{(25c)} \end{cases}$$

where the functions f_1, f_2 and f_3 are given by

$$\begin{cases} f_1\left(\phi_1, \phi_2, \phi_3\right) = \left(-\dfrac{\lambda_y}{2}\phi_1 + \omega_y^2 S_d \phi_2\right) & \text{(26a)} \\ f_2\left(\phi_1, \phi_2, \phi_3\right) = -\dfrac{1}{2j}\left(-\dfrac{j\omega_y S_c}{4\omega_\delta}\phi_1 + (\omega_\delta + 2\sigma + j\lambda_\delta)\phi_2 - \omega_\delta \phi_3\right) & \text{(26b)} \\ f_3\left(\phi_1, \phi_2, \phi_3, \epsilon\right) = -\dfrac{\omega_\delta^2}{\mu - 2j\omega_\delta}\phi_2 + \dfrac{\omega_\delta^2 - \alpha_1 + j\mu\omega_\delta}{\mu - 2j\omega_\delta}\phi_3 - \dfrac{3\alpha_3}{\mu - 2j\omega_\delta}\phi_3 \left|\phi_3\right|^2 \\ -\dfrac{\epsilon}{\mu - 2j\omega_\delta}\left(\dfrac{j\omega_y(T_c + S_c)}{4}\phi_1 + \left(\omega_\delta^2 - j\lambda_\delta\omega_\delta\right)\phi_2 + \left(\omega_\delta^2 + \alpha_1 - 2\sigma\omega_\delta - j\mu(\omega_\delta + \sigma)\right)\phi_3 + 3\alpha_3\phi_3\left|\phi_3\right|^2\right) & \text{(26c)} \end{cases}$$

Note that Ω has been replaced by

$$\Omega = \omega_y + \omega_\delta + \epsilon\sigma, \tag{27}$$

introducing the detuning term σ (with $\sigma \sim O(1)$) to analyze the system for Ω around $\omega_y + \omega_\delta$. Eqs. (25) describe the slow-flow of the RefM (12) and fixed points of this slow-flow trivially characterize periodic responses of the RefM model. It will be called the Reduced Model (RedM).

4.2 Geometric singular perturbation analysis

Eqs. (25) can be transformed by switching from the *slow* time scale t to the *super-slow* time scale $\tau = \epsilon t$ as

$$\begin{cases} \phi_1' = f_1\left(\phi_1, \phi_2, \phi_3\right) & \text{(28a)} \\ \phi_2' = f_2\left(\phi_1, \phi_2, \phi_3\right) & \text{(28b)} \\ \epsilon\ \phi_3' = f_3\left(\phi_1, \phi_2, \phi_3, \epsilon\right), & \text{(28c)} \end{cases}$$

where " $'$ " denotes the derivative with respect to time τ.

Eqs. (25) and (28) highlight the "slow/fast" nature of the system (recalling that ϵ is small). In this paper, we prefer to use the terminology introduced by Gendelman and Bar [6] for which the terms *fast* and *slow* are replaced by *slow* and *super-slow* respectively, whereby the term *fast* is reserved for the fast component $e^{j\omega_y t}$. Therefore, (25) and Eqs. (28) consist of one *slow* complex variable ϕ_3 and two *super-slow* complex variables ϕ_1 and ϕ_2. As already mentioned, Eq. (25) is the slow-flow of the system written at the time scale t.

Some of steps that have been developed to obtain equivalently Eqs. (25) (or (28)) are very hard to justify mathematically. So it will be important to numerically verify that the behaviors of the solutions captured by RedM is also observed with the complete model RefM.

4.2.1 Definition of the Critical Manifold

Solutions of Eqs. (25) (or equivalently (28)), can exhibit slow and super-slow epochs characterized by the speed at which the solution advances. The *Geometric Singular Perturbation Theory*

(GSPT) [34, 35, 36] is used to describe these dynamics for $0 < \epsilon \ll 1$. To achieve that, stating $\epsilon = 0$, Eqs. (25) and (28) are reduced respectively to the *slow subsystem*

$$\begin{cases} \dot{\phi}_1 = 0 & \text{(29a)} \\ \dot{\phi}_2 = 0 & \text{(29b)} \\ \dot{\phi}_3 = f_3\left(\phi_1, \phi_2, \phi_3, 0\right), & \text{(29c)} \end{cases}$$

and to the *super-slow subsystem*

$$\begin{cases} \phi_1' = f_1\left(\phi_1, \phi_2, \phi_3\right) & \text{(30a)} \\ \phi_2' = f_2\left(\phi_1, \phi_2, \phi_3\right) & \text{(30b)} \\ 0 = f_3\left(\phi_1, \phi_2, \phi_3, 0\right). & \text{(30c)} \end{cases}$$

Then, we use the following result of the GSPT: if $0 < \epsilon \ll 1$, the dynamics of the system during slow (resp. super-slow) epoch is given by the dynamic of the slow subsystem (29) (resp. super-slow subsystem (30)).

The so-called *Critical Manifold* (CM) [35] associated to Eqs. (29) and (30) is defined by the algebraic equation (30c) as

$$CM := \left\{(z_1, z_2, z_3) \in \mathbb{C}^3 \mid f_3\left(z_1, z_2, z_3, 0\right) = 0\right\}. \tag{31}$$

The CM is the set of the fixed points of the slow subsystem Eqs. (29) and it is also the subspace where the trajectories of Eqs. (30) take place.

From the expression of the function f_3, the CM takes the form

$$\phi_2 = \phi_3 F\left(|\phi_3|\right), \ \forall \phi_1, \tag{32}$$

where the complex-valued function F of a real positive variable is given by

$$F(x) = F_R(x) + jF_I(x) = 1 - \frac{\alpha_1}{\omega_\delta^2} - \frac{3\alpha_3}{\omega_\delta^2}x^2 + j\frac{\mu}{\omega_\delta}. \tag{33}$$

Note that the CM only depends on the resonance frequency of the blades and the damping and the cubic spring constant of the NES.

The structure of the CM as defined by Eqs. (32) and (33) has the same form as the structure of the CM obtained in [26] considering only one NES on the fuselage replacing the resonance frequency ω_y associated to the fuselage motion by the resonance frequency ω_δ associated to the lag motion. Moreover, this structure is similar to the structure of the CM obtained by Starosvetsky and Gendelman [4][3] studying harmonic forced vibration of one DOF linear system coupled to a NES and also in [10, 6] studying a nonlinear self-excitated system coupled to a NES. In [4, 10, 6] the studied systems involve only two DOF therefore the CM is defined in $\mathbb{C}^2$. The distinctive feature of this work is the fact that the system involves three DOF and hence the CM is defined in $\mathbb{C}^3$, keeping an equivalent form in the (ϕ_3, ϕ_2)-space.

The CM can be analyzed in the real domain. To achieve this, polar coordinates are introduced

$$\phi_1 = N_1 e^{j\theta_1}, \qquad \phi_2 = N_2 e^{j\theta_2} m \qquad \text{and} \qquad \phi_3 = N_3 e^{j\theta_3}. \tag{34}$$

and we compute successively the module and the argument of (32), that lies to

[3] In the reference [4] the critical manifolds is called *Slow Invariant Manifold*.

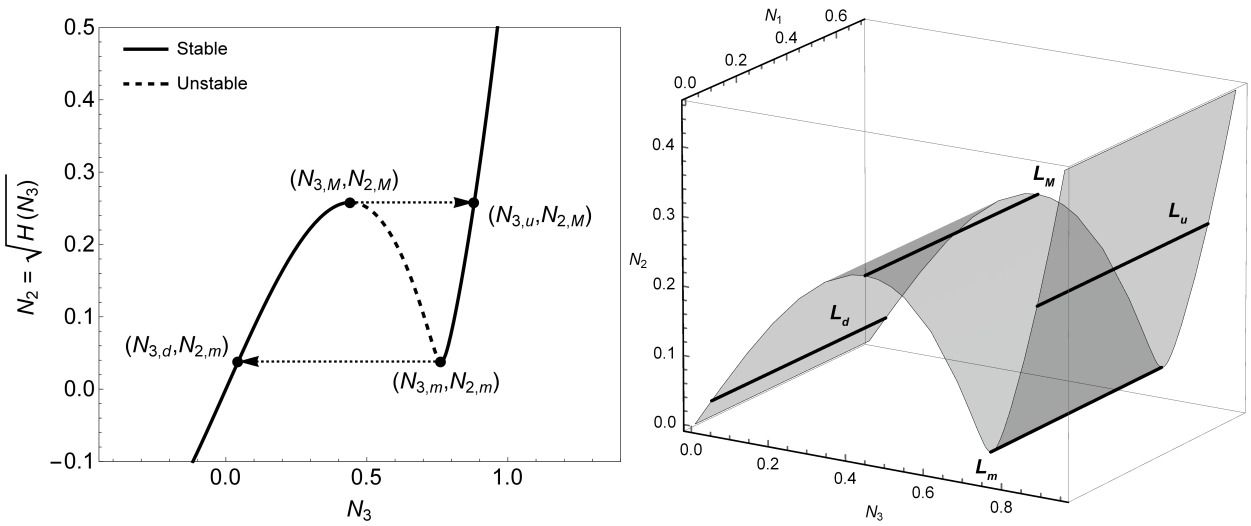

(a) (b)

Figure 4: *Critical Manifold* (CM). Following parameters are used: $\omega_\delta = 2$, $\alpha_1 = 0.5$, $\alpha_3 = 2$ and $\mu = 0.1$. (a) In the (N_3, N_2)-plane and (b) In the (N_3, N_2, N_1)-space.

$$\begin{cases} N_2^2 = H(N_3), & \text{(35a)} \\ \theta_2 = \theta_3 + \arctan\left(\dfrac{F_I(N_3)}{F_R(N_3)}\right), & \text{(35b)} \end{cases}$$

where

$$H(x) = x^2\left[F_R(x)^2 + F_I(x)^2\right], \tag{36}$$

is a real-valued function.

The shape of the CM in the (N_3, N_2)-plane depends on the existence of local extrema of the function H. The local extrema of the function $H(x)$ are given by the positive roots of its derivative $H'(x)$. An easy calculus shows that two local extrema occur at

$$N_{3,M} = \frac{1}{3}\sqrt{\frac{2\left(\omega_\delta^2 - \alpha_1\right) + \sqrt{\left(\omega_\delta^2 - \alpha_1\right)^2 - 3\mu^2\omega_\delta^2}}{\alpha_3}} \tag{37}$$

$$N_{3,m} = \frac{1}{3}\sqrt{\frac{2\left(\omega_\delta^2 - \alpha_1\right) - \sqrt{\left(\omega_\delta^2 - \alpha_1\right)^2 - 3\mu^2\omega_\delta^2}}{\alpha_3}}, \tag{38}$$

if the following relation holds

$$\mu < \frac{1}{\sqrt{3}}\frac{\omega_\delta^2 - \alpha_1}{\omega_\delta}, \tag{39}$$

and in this case $N_{3,M} < N_{3,m}$. This situation is illustrated Fig. 4(a). Including the third variable ϕ_1 as N_1, the CM is a surface in the 3D-space plotted Fig. 4(b).

4.2.2 *Stability analysis on Critical Manifold*

Stability analysis of the CM can be performed in terms of fixed points of the slow subsystem (29). As in [4], it can be shown that the stability condition of the CM is equivalent to

$$H'(N_3) > 0. \tag{40}$$

Hence the stability range of the CM is characterized by the points $(N_{3,m}, N_{2,m})$ and $(N_{3,M}, N_{2,M})$ where

$$N_{2,M} = \sqrt{H(N_{3,M})} \text{ and } N_{2,m} = \sqrt{H(N_{3,m})} \tag{41}$$

which are therefore called *fold points* [37]. At each fold point it is associated a landing point, $(N_{3,d}, N_{2,m})$ and $(N_{3,u}, N_{2,M})$ respectively, where $N_{3,d}$ and $N_{3,u}$ are solutions of

$$H(N_{3,d}) = H(N_{3,m}) \text{ and } H(N_{3,u}) = H(N_{3,M}) \tag{42}$$

respectively.

A typical *Critical Manifold* and it stability range are depicted in (N_3, N_2)-plane (see Fig. 4(a)) and in the (N_3, N_2, N_1)-space (see Fig. 4(b)). In the (N_3, N_2, N_1)-space, each fold point defines a folded line (L_M and L_m) co-linear to the N_1-axis. The points $N_{3,d}$ and $N_{3,u}$ define respectively the line L_d and L_u which are also co-linear to the N_1-axis.

4.2.3 *Steady-state regimes*

The shape and the stability property of the CM (i.e. the existence of folded lines on which the stability of the CM changes) shown in Fig. 4 allows to define at least three steady-state regimes of the RedM model (25) in coherence with the steady-state response regimes described in Sect. 3.2.

To describe the steady regimes of the slow flow we consider situations on which, after an transient regime, the trajectory of the system arrives at a point M_0 on the CM. After that, three steady-state regimes may be considered:

A fixed point of the RedM is reached. These situations corresponds to a periodic solutions of the RefM. Note that to have equivalence between fixed point of the RedM and Periodic Solutions (PR) of the RefM, the RedM must be written using polar coordinates and argument differences must be considered, see Appendix A of [26] for more details.

Relaxation oscillations. The S-shape of the CM in the (N_3, N_2)-plane suggests also the possible existence of *relaxation oscillations* [38]: from M_0 the system reaches a point $S_0 \in L_M$, jumps to a point $S_1 \in L_u$ and undergoes a super-slow evolution (in the stable domain of the CM) until it reaches a point $S_2 \in L_m$. After another jump from S_2 to $S_3 \in L_u$ and a super-slow evolution (in the stable domain of the CM), the trajectory of the system returns to $S_0 \in L_M$. Such scenario of relaxation oscillations for the slow-flow can explain the existence of *Strongly Modulated Responses* [10, 6, 4] (SMR) for the RefM. Note that if $\mu > \frac{1}{\sqrt{3}} \frac{\omega_\delta^2 - \alpha_1}{\omega_\delta}$, the S-shape nature of the CM is lost and therefore relaxation oscillations are note possible.

Explosion. Until a first jump the slow-flow evolves the same way as for relaxation oscillations mechanism. However, instead of moving toward a stable fixed point or the folded line L_m, the trajectory of the system follows the CM to the infinity. This scenario explains *no suppression* regime for the RefM.

The existence of one of the three steady-state regimes described above (or an other) depends of the position and the stability of the fixed points of the RedM (25). Indeed, a stable fixed point

of the RedM placed on the stable part of the CM is a necessary condition to obtain PR of the RefM (12). On the other hand, the relaxation oscillations of the RedM (i.e SMR for the RefM) can exist if both folded lines L_M and L_m have attractive parts. Position and stability of the fixed points of Eq. (25) and attractivity (or repulsively) of the folded lines are determined through the study of the super-slow subsystem (30).

4.2.4 Super-slow subsystem analysis

Introducing the CM Eq. (32) in Eqs. (30a) and (30b), the super-slow subsystem is written only with respect to the variables ϕ_1 and ϕ_3

$$\begin{cases} \dfrac{d\phi_1}{d\tau} = f_1\left(\phi_1, \phi_3 F\left(|\phi_3|\right), \phi_3\right) & \text{(43a)} \\ \dfrac{d\left[\phi_3 F(|\phi_3|)\right]}{d\tau} = f_2\left(\phi_1, \phi_3 F\left(|\phi_3|\right), \phi_3\right). & \text{(43b)} \end{cases}$$

Using the polar coordinates (34) and separating real and imaginary parts, Eqs. (43) can be finally reduced (after some calculation steps) to the following form

$$\begin{cases} g(N_3)\dfrac{dN_3}{d\tau} = f_{N_3}\left(N_1, N_3, \delta_{31}\right) & \text{(44a)} \\ g(N_3)\dfrac{d\delta_{31}}{d\tau} = f_{\delta_{31}}\left(N_1, N_3, \delta_{31}\right) & \text{(44b)} \\ \dfrac{dN_1}{d\tau} = f_{N_1}\left(N_1, N_3, \delta_{31}\right), & \text{(44c)} \end{cases}$$

where

$$g(x) = \frac{H'(x)}{2}. \tag{45}$$

From Eqs. (44), it is possible to detect *fixed points* and *folded singularities*. The (regular) fixed points of Eqs. (44), $\{N_1^e, N_3^e, \delta_{31}^e\}$, are defined by as

$$\begin{aligned} f_{N_3}\left(N_1^e, N_3^e, \delta_{31}^e\right) &= 0, & \text{(46a)} \\ f_{\delta_{31}}\left(N_1^e, N_3^e, \delta_{31}^e\right) &= 0, & \text{(46b)} \\ f_{N_1}\left(N_1^e, N_3^e, \delta_{31}^e\right) &= 0 & \text{(46c)} \\ g(N_3^e) &\neq 0. & \text{(46d)} \end{aligned}$$

If $\epsilon \ll 1$, fixed points computed from Eqs. (46) corresponds to fixed points of the RedM model (25). As usual, stability of the fixed points are found by looking the sign of the eigenvalues real parts of the Jacobian matrix of the vector function $\mathbf{F_2} = (f_{N_3}/g, f_{\delta_{31}}/g, f_{N_1})$ evaluated at $\{N_1^e, N_3^e, \Delta_{31}^e\}$. From this, a theoretical bifurcation diagram can be obtained showing amplitudes and stability range of the fixed point (resp. periodic regimes) of the RedM (25) (resp. RefM (12)) with respect of the detuning term σ.

As a remark, Eqs. (44) have the same form that the equivalent equations obtained when one NES is attached on fuselage (see Eq. (68) of [26]). In the previous cited paper, detailed analysis Eqs. (44) is proposed. In particular, folded singularities, which are signs of SMR in the system and gives indications about attractivity (or repulsively) of the folded lines are highlighted and computed. This analysis is not recalled here.

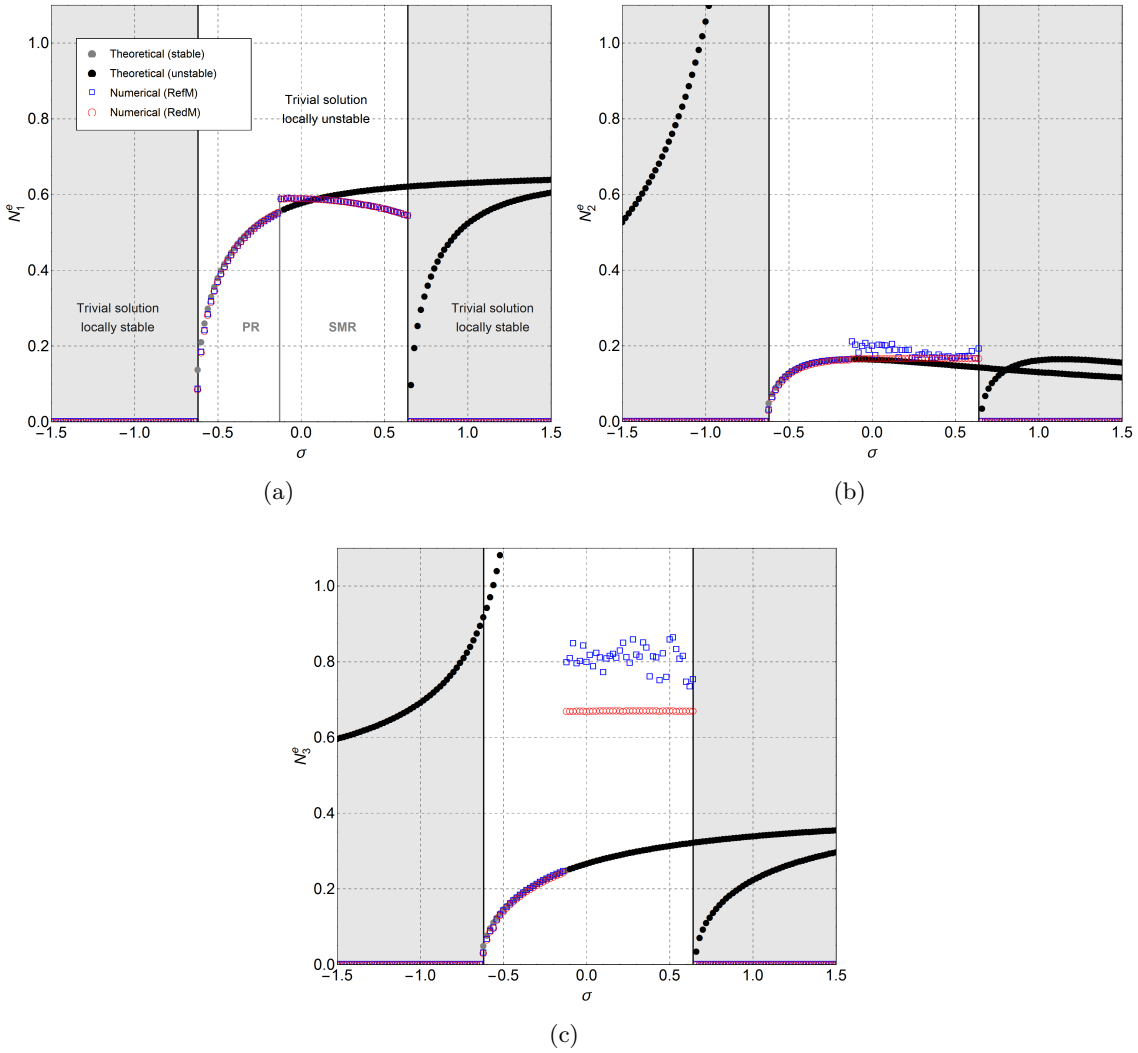

Figure 5: Comparison between theoretical bifurcation diagram, obtained from Eq. (46) (gray dots stable fixed points and black dots for unstable fixed points) and maximum steady-state amplitudes obtained from numerical simulations of the RefM (12) (blue squares) and from numerical simulations of the RedM model (25) (red circles). Bifurcation diagram and maximum steady-state amplitudes are plotted for the variables (a) N_1, (b) N_2 and (c) N_3 as a function of σ. When the trivial solution is unstable, parameter range in which PR or SMR are observed are specified on the figure. The parameters used are: $\lambda_y = 0.3$, $\omega_y = 1$, $\lambda_\delta = 0.2$, $\omega_\delta = 2$, $S_d = 1$, $T_d = 1$, $S_c = 2$, $T_c = 2$, $\mu = 0.1$, $\alpha_1 = 0.05$, $\alpha_3 = 7$ and $\epsilon = 0.01$.

5 Benchmark of theoretical results and discussion

In this section, a bifurcation analysis deduced from the theoretical results discussed in previous section is compared with a bifurcation analysis obtained from numerical integration of the RefM model (12) and of the RedM model (25). The comparison between numerical simulations of RefM and RedM (i.e. the slow-flow) is important because the capacity of the RedM to reproduce the behavior of RefM reflect the validity and quality of all mathematical developments which derive from (even those not presented in this paper). It is important to note that the NES is not subject to an optimization. The parameters used in this section are chosen to illustrate with only two sets of parameters the potential of the NES to modify the response regime after the bifurcation of the trivial solution.

The detuning parameter σ is used as the bifurcation parameter. For each given σ, the solver NDSolve available in Mathematica is used to solve the ordinary differential equations ((12) and (25))

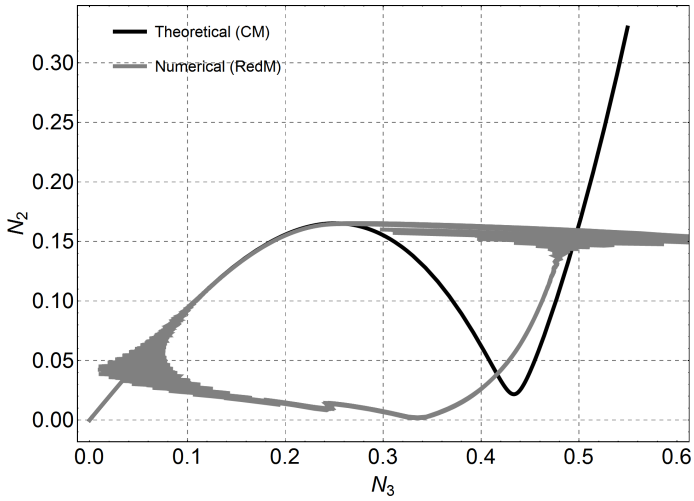

Figure 6: Comparison between the trajectory of the simulated RedM (25) in the plane (N_3, N_2) and the *Critical Manifold* (35a). Parameters and initial conditions are the same as for Fig. 5 with $\sigma = 0$.

over $[0, T]$ with large T (long time integration to reach the steady state regime) with the following options: `MaxSteps` $\rightarrow$ `Infinity`, `AccuracyGoal` $\rightarrow$ `Automatic`, `PrecisionGoal` $\rightarrow$ `Automatic`, `WorkingPrecision` $\rightarrow$ `MachinePrecision`. The steady state-regimes are characterized by the maximum amplitude of the considered signal evaluated on the end time interval $[T - T_{ss}, T]$ (with $T_{ss} \ll T$). Numerical bifurcation diagrams are then built starting from the smaller value of σ solving the ordinary differential equations with initial conditions as a small perturbation of the trivial solution and next increasing σ and solving the ordinary differential equations with initial conditions corresponding to the steady-state regimes obtained for the previous value of σ.

A first comparison is shown in Fig. 5 where the bifurcation diagrams associated to the three variables N_1 (Fig. 5(a)), N_2 (Fig. 5(b)) and N_3 (Fig. 5(c)) are plotted for $\sigma \in [-1.5, 1.5]$ (see Fig. 5 caption to know the used parameters). The chosen set of parameters (see Fig. 5 caption) has been used to illustrate the suppression of the GR instability over a whole σ-interval $[-1.5, 1.5]$. The corresponding numerical values of the parameters characterizing the RefM model (12) are deduced from (13), they are not reported here.

First of all, it interesting to note that the responses obtained by numerical integrations of Eqs. (12) and Eqs. (25) are very close. Moreover, these responses are also very close to the responses predicted by the analytical method when the stability criterion is satisfied i.e for $-1.5 \leq \sigma \leq -0.13$ and $0.64 \leq \sigma \leq 1.5$ (Fig. 5, gray dot markers). We can observe that, starting from $\sigma = -1.5$, the transition from *complete suppression of GR instability* to *partial suppression through PR* occurs when the trivial solution loses its stability (at $\sigma \approx -0.6$, numerical value given by the theoretical approach). In the same way, the transition from *partial suppression through PR* to *partial suppression through SMR*, manifested as a jump of the steady-state amplitudes of the numerical simulations, occurs when the stable fixed points of the RedM lose their stability (at $\sigma \approx -0.13$, numerical value given by the theoretical approach). For $-0.13 < \sigma < 0.64$, fixed points of the RedM are unstable and SMR are observed on numerical simulations. Finally, for $\sigma > 0.64$ (numerical value given by the theoretical approach), the trivial solution get its stability back and *complete suppression* is again observed on numerical simulations for both RefM and RedM.

To complete this first comparative study, a trajectory of the RedM (25) when SMR occurs is plotted, Fig. 6, in the (N_3, N_2)-plane and compared to the *Critical Manifold* given by Eq. (35a). The numerical value $\sigma = 0$ is used. This simulation illustrates the relaxation oscillations scenario.

These results illustrate how the analytical approach is able to predict different types of steady state regimes and explain the suppression mechanism. However, two comments have to be made on

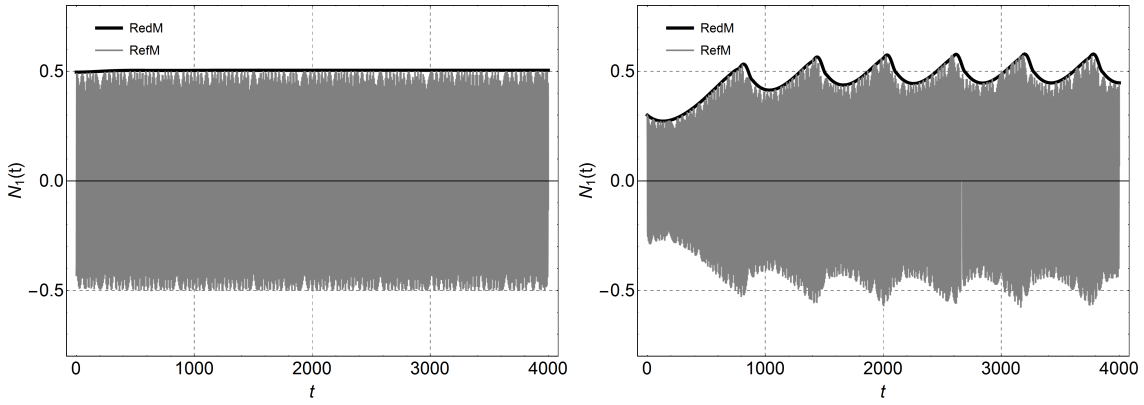

Figure 7: Comparison between numerical integration of the RefM (12) (gray line) and of the RedM model (25) (black line). The parameters are the same as for Fig. 5 with $\sigma = -0.3$ and two set of initial condition are used: (a) the systems are initialized close to its stable steady-state regime (fixed point for the RedM and PR for the RefM), (b) the initial conditions are: $y(0) = 0.3$ for the RefM and $\phi_1(0) = j0.3$ for the RedM, all others initial conditions are equal to zero.

the limitation of the proposed procedure. The first point concerns the existence of the SMR. The proposed procedure allows finding only necessary conditions for the SMR and does not give any sufficient condition as it time-invariant done for example in [4] considering external forced systems problem or for example in [6] considering self-excited systems. Indeed, in works in which the super-slow flow subsystem can be reduced to a one-dimensional system [39, 10, 6], global structure of possible response regimes can be deduced from the linear stability analysis of the slow-flow (i.e. the RedM). In our study, the super-slow subsystem (44) is a three-dimensional system. In this case, the linear stability analysis is not sufficient to predict unequivocally the nature of the steady-state response regimes. Indeed, depending of the initial conditions, a stable fixed point of the RedM in the (δ_{31}, N_3, N_1)-space can never be reached. The second point concerns the co-existence of distinct stable steady-state responses. The nature of the steady-state response regimes (PR or SMR) depends of the stability of the fixed points of the RedM but also of their basin of attraction. In the example of Fig. 5 the basin of attraction of the stable fixed points reduces when σ approaches the transition value $\sigma \approx -0.13$. Consequently the transition from *partial suppression through PR* to *partial suppression through SMR* may occur at a smaller value than that which corresponds to the loss of stability of the fixed point of the slow-flow. This is illustrated in Fig. 7. Indeed, in Fig. 7(a), the RefM and RedM are initialized with initial conditions close to the stable steady-regime and the expected responses (periodic regime for the RefM and fixed point for the RedM) are actually observed. In Fig. 7(b), other initial conditions are chosen (see figure caption the exact value) and SMR is observed even if the fixed point of the RedM is stable. These previous observations highlight that situations in which a competition between a stable fixed point and a stable relaxation oscillations cycle of the slow-flow can occur. Similar problems due to the relatively high dimension of the system was already encountered in previous study by the authors [26] and also when a NES is used as a passive control device for a nonlinear elastic string, in internal resonance conditions, excited by an external harmonic force [40].

A second comparison is shown in Fig. 8 considering the same set of numerical values except for $\lambda_y = 0.3$, $S_d = 1$, $\alpha_1 = 0.05$ and $\alpha_3 = 7$. For this set of values, the suppression of the GR instability is not satisfied over the whole σ-interval $[-3, 3]$. As in Fig. 5, starting from $\sigma = -3.$, the transition from *complete suppression of GR instability* to *partial suppression through PR* occurs when the trivial solution loses its stability (at $\sigma \approx -1.8$, numerical value given by the theoretical approach).

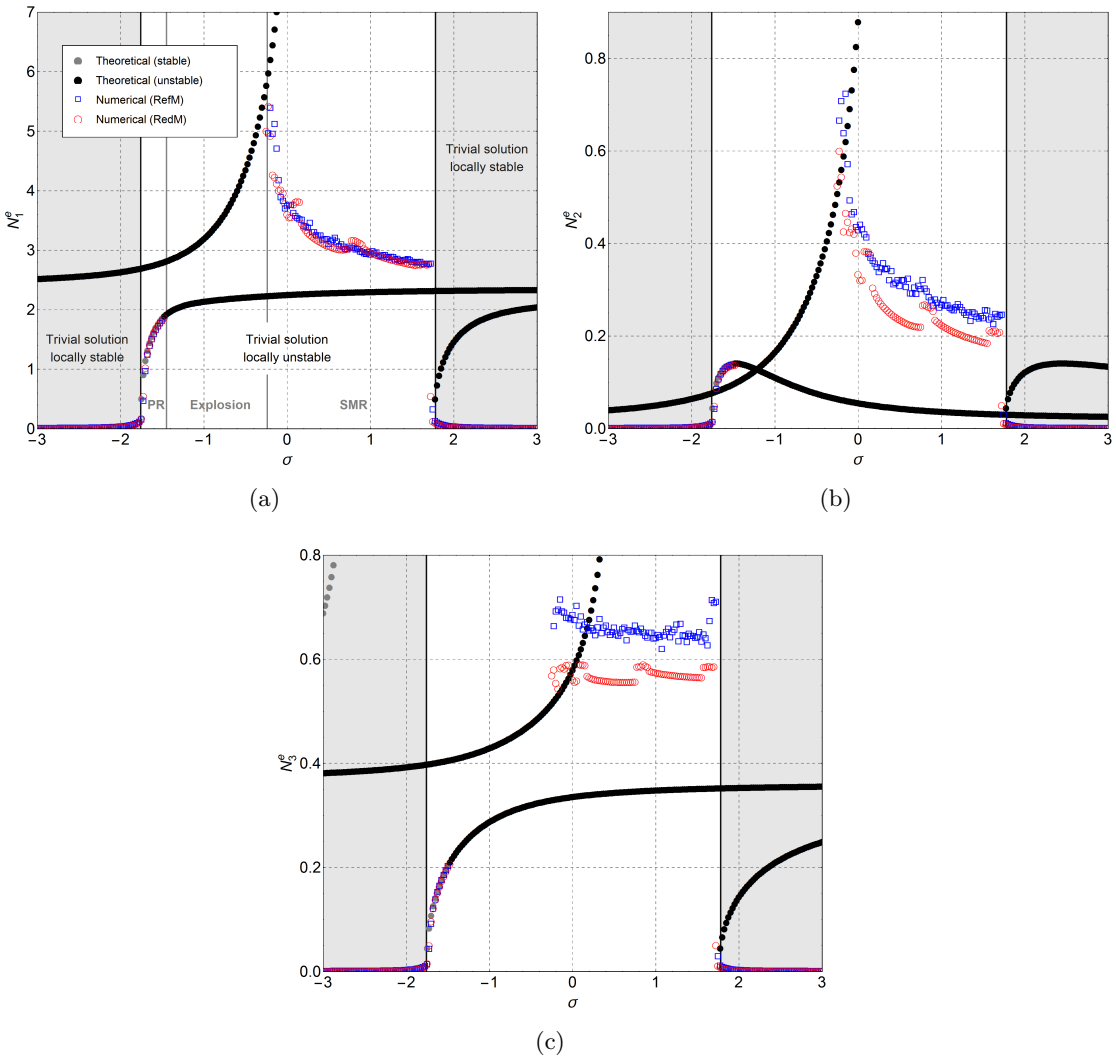

Figure 8: Comparison between theoretical bifurcation diagram, obtained from Eq. (46) (gray dots stable fixed points and black dots for unstable fixed points) and maximum steady-state amplitudes obtained from numerical simulations of the RefM (12) (blue squares) and from numerical simulations of the RedM model (25) (red circles). Bifurcation diagram and maximum steady-state amplitudes are plotted for the variables (a) N_1, (b) N_2 and (c) N_3 as a function of σ. When the trivial solution is unstable, parameter range in which PR SMR or Explosion are observed are specified on the figure. The parameters used are: $\lambda_y = 0.075$, $\omega_y = 1$, $\lambda_\delta = 0.2$, $\omega_\delta = 2$, $S_d = 4$, $T_d = 1$, $S_c = 2$, $T_c = 2$, $\mu = 0.1$, $\alpha_1 = 0$, $\alpha_3 = 10$ and $\epsilon = 0.01$.

Partial suppression through PR is satisfied up to $\sigma \approx -1.45$, where the stable fixed points of the RedM lose their stability. For $\sigma > 1.8$ (numerical value given by the theoretical approach), the trivial solution get its stability back and *complete suppression* is again observed. Finally, for $-1.45 \leq \sigma \leq 1.8$, numerical simulations show responses with *partial suppression through SMR* and responses with *no suppression of GR*. Unfortunately, the theoretical bifurcation diagram does not give elements to discriminate SMR, the reason is also the fact that the super-slow subsystem (44) is a three-dimensional system.

As a final remark, to conclude unequivocally about the nature of the steady-state response of the system for a given set of parameters and a given set of initial conditions two informations are missing: the stability range of the relaxation oscillations and the size of the basins of attraction of the stable solutions. This may be subject of future work.

6 About the comparison between blade and fuselage NES attachments

The configuration using NES on the fuselage (as presented in [26]) and configuration using NES attached directly on the blades (as presented here) have the same potential to mitigate GR instability.

This section does not present a rigorous comparison between the two configurations but only few words about it are expounded. The reason is the fact that the efficiency of a NES depends of its design. Therefore, the comparison between NES attached on the fuselage and NES attached on the blades depends more, in our view, on the technical implementation of each solution, which is not the purpose of the paper. However, the blade NES attachments leave more possibilities for engineers for a possible implementation because in this case the small dimensionless parameter depends on both the mass ratio and the squared length ratio between the NES and the blades. Regarding to the fuselage NES attachment configuration in which the small dimensionless parameter depends only on the mass ratio between the NES and the fuselage.

7 Conclusion

We studied the response of a ground resonance helicopter model including ungrounded NES attached on the blades of the engine. An helicopter model involving fuselage, blades and the cubic NES dynamics was reduced applying a complex multi-blade transformation to the blades and to the NES, defining the Reference Model (RefM).

As usual, in the framework of NES properties exploration and particularly in the context of dynamic instabilities mitigation, four steady-state response regimes were highlighted: complete suppression, partial suppression through periodic response, partial suppression through strongly modulated response and no suppression of the GR instability.

The first regime corresponds to the local stability of the trivial solution of the RefM. To explain all the regimes the slow-flow of the system is determined using complexification-averaging (CA-X). The presence of a small dimensionless parameter related to the moments of inertia of the NES in the slow-flow system implies that it involves one "slow" complex variable and two "super-slow" complex variables. The "super-slow/slow" nature of the system allowed us to use the so-called geometric singular perturbation theory to analyze it.

In particular, the Critical Manifold of the slow-flow was determined as well as its theoretical bifurcation diagram which predicts the possible periodic responses of the RefM et their stability. The S-shape of the Critical Manifold, involving two folded lines, and the associated stability properties provide an analytical tool to explain the existence of three regimes: periodic response regimes, strongly modulated response regimes and no suppression regimes which appear when the trivial solution is unstable. Moreover, the theoretical bifurcation diagram gives indications about the nature the steady-state responses of the system. However, because the super-slow flow subsystem cannot be reduced to a one-dimensional system, the nature the steady-state responses cannot be predicted unequivocally. Indeed, two informations are missing: the stability range of the SMR and the size of the basins of attraction of the stable solutions. This may be subject of future work.

Acknowledgements

This research was done within the framework of the industrial chair "Dynamique des Systèmes Mécaniques Complexes (*Dynamics of complex mechanical systems*)" financed by the *Airbus Group Foundation*.

References

[1] A. Vakakis, O. Gendelman, Energy pumping in nonlinear mechanical oscillators: Part II - Resonance capture, Journal of Applied Mechanics 68 (2001) 42–48.

[2] E. Gourdon, N. Alexander, C. Taylor, C. Lamarque, S. Pernot, Nonlinear energy pumping under transient forcing with strongly nonlinear coupling: Theoretical and experimental results, Journal of Sound and Vibration 300 (2007) 522–551.

[3] A. F. Vakatis, O. V. Gendelman, L. A. Bergman, D. M. McFarland, G. Kerschen, Y. S. Lee, Nonlinear Targeted Energy Transfer in Mechanical and Structural Systems, Springer-Verlag, Berlin, New York, 2008.

[4] Y. Starosvetsky, O. V. Gendelman, Strongly modulated response in forced 2dof oscillatory system with essential mass and potential asymmetry, Physica D 237 (13) (2008) 1719–1733. doi:10.1016/j.physd.2008.01.019.

[5] Y. S. Lee, A. F. Vakakis, L. A. Bergman, D. M. McFarland, Suppression of limit cycle oscillations in the van der Pol oscillator by means of passive non-linear energy sinks, Structural Control and Health Monitoring 13 (1) (2006) 41–75. doi:10.1002/stc.143.

[6] O. V. Gendelman, T. Bar, Bifurcations of self-excitation regimes in a Van der Pol oscillator with a nonlinear energy sink, Physica D 239 (3-4) (2010) 220–229. doi:10.1016/j.physd.2009.10.020.

[7] Y. S. Lee, A. F. Vakakis, L. A. Bergman, D. M. McFarland, G. Kerschen, Suppression aeroelastic instability using broadband passive targeted energy transfers, part 1: Theory, AIAA Journal 45 (3) (2007) 693–711. doi:10.2514/1.24062.

[8] Y. S. Lee, A. F. Vakakis, L. A. Bergman, D. M. McFarland, G. Kerschen, Suppression aeroelastic instability using broadband passive targeted energy transfers, part 2: Experiments, AIAA Journal 45 (3) (2007) 2391–2400. doi:10.2514/1.24062.

[9] Y. S. Lee, A. Vakakis, L. Bergman, D. McFarland, G. Kerschen, Enhancing the robustness of aeroelastic instability suppression using multi-degree-of-freedom nonlinear energy sinks, AIAA Journal 46 (6) (2008) 1371–1394.

[10] O. Gendelman, A. Vakakis, L. Bergman, D. McFarland, Asymptotic analysis of passive nonlinear suppression of aeroelastic instabilities of a rigid wing in subsonic flow, SIAM Journal on Applied Mathematics 70 (5) (2010) 1655–1677. doi:10.1137/090754819.

[11] B. Vaurigaud, L. Manevitch, C.-H. Lamarque, Passive control of aeroelastic instability in a long span bridge model prone to coupled flutter using targeted energy transfer, Journal of Sound and Vibration 330 (2011) 2580–2595.

[12] A. Luongo, D. Zulli, Aeroelastic instability analysis of nes-controlled systems via a mixed multiple scale/harmonic balance method, Journal of Vibration and Control 20 (13) (2014) 1985–1998.

[13] A. Nankali, Y. S. Lee, T. Kalmar-Nagy, Suppression of regenerative instabilities by means of targeted energy transfers, in: A. Adams, G. Kerschen, A. Carrella (Eds.), Topics in Nonlinear Dynamics, Volume 3, 2012, pp. 181–190.

[14] E. Gourc, S. Sguy, G. Michon, A. Berlioz, B. Mann, Quenching chatter instability in turning process with a vibro-impact nonlinear energy sink, Journal of Sound and Vibration 355 (2015) 392–406.

[15] R. Viguié, G. Kerschen, J. Golinval, D. McFarland, L. Bergman, A. Vakakis, N. van de Wouw, Using passive nonlinear targeted energy transfer to stabilize drill-string systems, Mechanical Systems and Signal Processing 23 (2009) 148–169.

[16] G. Habib, G. Kerschen, Suppression of limit cycle oscillations using the nonlinear tuned vibration absorber, Proceedings of the Royal Society A 471 (2176).

[17] R. P. Coleman, A. M. Feingold, Theory of self excited mechanical oscillations of helicopter rotor with hinged blades, Tech. rep., NACA Report 1351 (1958).

[18] W. Johnson, Helicopter theory, Dover publications, inc., 1994.

[19] A. R. S. Bramwell, D. Balmford, G. T. S. Done, Bramwell's helicopter dynamics, 2001.

[20] D. Kunz, Nonlinear analysis of helicopter ground resonance, Nonlinear Analysis: Real World Applications 3 (2002) 383–395.

[21] T. Krysinski, F. Malburet, Instabilité mécanique: contrôle actif et passif, Lavoisier, 2009.

[22] L. Sanches, G. Michon, D. Berlioz, A.and Alazard, Parametrically excited helicopter ground resonance dynamics with high blade asymmetries, Journal of Sound and Vibration 331 (16) (2012) 3897–3913.

[23] G. T. S. Done, A simplified approach to helicopter ground resonance, Aeronautical Journal 78 (761) (1974) 204–208.

[24] D. Tang, E. Dowell, Influence of nonlinear blade damping on helicopter ground resonance instability, Journal Aircraft 23 (2) (1986) 104–110.

[25] G. Quaranta, V. Muscarello, P. Masarat, Lead-lag damper robustness analysis for helicopter ground resonance, Journal of Guidance, Control, and Dynamics 36 (4) (2013) 1150–1161.

[26] B. Bergeot, S. Bellizzi, B. Cochelin, Analysis of steady-state response regimes of a helicopter ground resonance model including a non-linear energy sink attachment, International Journal of Non-Linear Mechanics 78 (2016) 72 – 89. doi:http://dx.doi.org/10.1016/j.ijnonlinmec.2015.10.006.
URL http://www.sciencedirect.com/science/article/pii/S0020746215002000

[27] B. Bergeot, S. Bellizzi, B. Cochelin, Passive suppression of helicopter ground resonance instability by means of a strongly nonlinear absorber, Advance in Aircraft and Spacecraft Science 3 (3) (2016) 271–298.

[28] S. Bab, S. E. Khadem, M. Shahgholi, Lateral vibration attenuation of a rotor under mass eccentricity force using non-linear energy sink, International Journal of Non-Linear Mechanics 67 (2014) 251–266. doi:10.1016/j.ijnonlinmec.2014.08.016.

[29] S. Bab, S. E. Khadem, M. Mahdiabadi, M. Shahgholi, Vibration mitigation of a rotating beam under external periodic force using a nonlinear energy sink (nes), Journal of Vibration and Control (2015) 1–25(First published on June 1, 2015).

[30] M.-R. Ghazavi, A. Najafi, A.-A. Jafari, Bifurcation and nonlinear analysis of nonconservative interaction between rotor and blade row, Mechanism and Machine Theory 65 (2013) 29–45. doi:10.1016/j.mechmachtheory.2013.02.008.

[31] A. H. Nayfeh, D. T. Mook, Nonlinear Oscillations, Wiley Classics Library, Wiley-VCH, 1995.

[32] A. H. Nayfeh, B. Balachandran, Applied nonlinear dynamics, Wiley Series in Nonlinear Science, Wiley-VCH, 1995.

[33] L. Manevitch, Complex representation of dynamics of coupled nonlinear oscillators, in: L. Uvarova, A. Arinstein, A. Latyshev (Eds.), Mathematical Models of Non-Linear Excitations, Transfer, Dynamics, and Control in Condensed Systems and Other Media, Springer US, 1999, pp. 269–300. doi:10.1007/978-1-4615-4799-0_24.

[34] N. Fenichel, Geometric singular perturbation theory for ordinary differential equations, Journal of Differential Equations 98 (1979) 53–98.

[35] C. Jones, Geometric singular perturbation theory, in: R. Johnson (Ed.), Dynamical Systems, Vol. 1609 of Lecture Notes in Mathematics, Springer Berlin Heidelberg, 1995, pp. 44–118. doi:10.1007/BFb0095239.

[36] M. Desroches, J. Guckenheimer, B. Krauskopf, C. Kuehn, H. Osinga, M. Wechselberger, Mixed-mode oscillations with multiple time scales, SIAM Review 52 (2) (2012) 211–288. doi:10.1137/100791233.

[37] R. Seydel, Practical Bifurcation and Stability Analysis, 3rd Edition, Vol. 5 of Interdisciplinary Applied Mathematics, Springer, 2010.

[38] J. Grasman, Asymptotic Methods for Relaxation Oscillations and Applications, Vol. 63 of Applied Mathematical Sciences, Springer-Verlag, 1987.

[39] E. Domany, O. Gendelman, Dynamic responses and mitigation of limit cycle oscillations in Van der Pol-Duffing oscillator with nonlinear energy sink, Journal of Sound and Vibration 332 (21) (2013) 5489–5507. doi:10.1016/j.jsv.2013.05.001.
URL http://linkinghub.elsevier.com/retrieve/pii/S0022460X13004069

[40] A. Luongo, D. Zulli, Nonlinear energy sink to control elastic strings: the internal resonance case, Nonlinear Dynamics 81 (1) (2015) 425–435. doi:10.1007/s11071-015-2002-8.
URL http://dx.doi.org/10.1007/s11071-015-2002-8